ACSNANO
www.acsnano.org
ARTICLE

Interfacial Degradation of Planar Lead Halide Perovskite Solar Cells

Antonio Guerrero,*[,†] Jingbi You,[‡] Clara Aranda,[†] Yong Soo Kang,[§] Germà Garcia-Belmonte,[†] Huanping Zhou,[‡] Juan Bisquert,[†,∥] and Yang Yang*[,‡]

[†]Institute of Advanced Materials (INAM), Universitat Jaume I, 12006 Castelló, Spain

[‡]Department of Materials Science and Engineering, University of California, Los Angeles, California 90095, United States

[§]Center for Next Generation Dye-sensitized Solar Cells, Department of Energy Engineering, Hanyang University, Seoul 133-791, South Korea

[∥]Department of Chemistry, Faculty of Science, King Abdulaziz University, Jeddah 21589, Saudi Arabia

S *Supporting Information*

ABSTRACT: **The stability of perovskite solar cells is one of the major challenges for this technology to reach commercialization, with water believed to be the major degradation source. In this work, a range of devices containing different cathode metal contacts in the configuration ITO/PEDOT:PSS/$MAPbI_3$/PCBM/Metal are fully electrically characterized before and after degradation caused by steady illumination during 4 h that induces a dramatic reduction in power conversion efficiency from values of 12 to 1.8%. We show that a decrease in performance and generation of the S-shape is associated with chemical degradation of the metal contact. Alternatively, use of Cr_2O_3/Cr as the contact enhances the stability, but modification of the energetic profile during steady illumination takes place, significantly reducing the performance. Several techniques including capacitance−voltage, X-ray diffraction, and optical absorption results suggest that the properties of the bulk perovskite layer are little affected in the device degradation process. Capacitance−voltage and impedance spectroscopy results show that the electrical properties of the cathode contact are being modified by generation of a dipole at the cathode that causes a large shift of the flat-band potential that modifies the interfacial energy barrier and impedes efficient extraction of electrons. Ionic movement in the perovskite layer changes the energy profile close to the contacts, modifying the energy level stabilization at the cathode. These results provide insights into the degradation mechanisms of perovskite solar cells and highlight the importance to further study the use of protecting layers to avoid the chemical reactivity of the perovskite with the external contacts.**

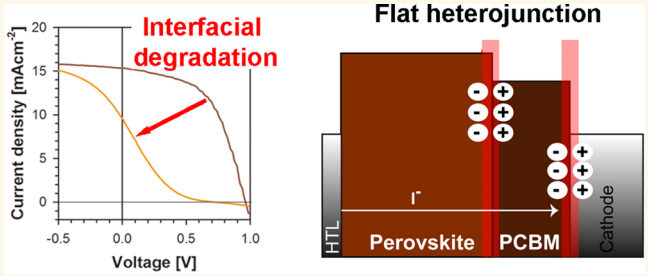

KEYWORDS: *perovskite photovoltaics, interfacial degradation, capacitance−voltage, impedance spectroscopy*

Photovoltaic applications based on perovskite materials as light harvesters are emerging technologies which have stirred the interest of both scientific and industrial communities.[1−3] Significant efforts have been devoted toward the achievement of high efficiencies using perovskites based on methylammonium lead triiodide ($MAPbI_3$), and impressive efficiencies as high as 20.1% have been obtained.[4] These recent developments demonstrate the enormous potential of perovskite solar cells, suggesting that they may soon compete with already commercially available photovoltaic technologies. However, in order for this technology to reach maturity, other aspects need to be resolved such as the long-term stability.

Stability of the devices depends on many factors such as the architecture or the employed deposition method. A variety of device configurations composed of different combinations of material layers have been proposed, and any instability arising from these materials will be critical for the device lifetime. Examples of architectures that have been developed are those consisting of a flat configuration based on ITO/TiO_2/Perovskite/Spiro-OMetad/Au, a variation with a porous layer of a metal oxide at the cathode contact, or an inverted configuration (ITO/PEDOT:PSS/Perovskite/PCBM/Al). Alternatively, several low-cost deposition methods are currently available as those regarded as preliminary techniques toward roll-to-roll technologies such as spin-coating,[3] doctor blade,[5] slot die, or screen printing.[6,7] Regarding the perovskite generation, this can be achieved by one-step solution coating,[2] two-step sequential dip-coating, or vapor phase deposition.[1,8]

Received: June 17, 2015
Accepted: December 17, 2015
Published: December 17, 2015

 © 2015 American Chemical Society

DOI: 10.1021/acsnano.5b03687
ACS Nano 2016, 10, 218−224

Water is believed to be the major degradation source for these types of devices. The mechanism is not totally understood, but it is clear that hybrid perovskites can react with Lewis bases such as water to irreversibly release methylammonium iodide and PbI_2. A degradation mechanism has been proposed by Frost *et al.*, where a single water molecule is sufficient to degrade the material.[9] However, an excess of water is required to dissolve the HI and CH_3NH_2 byproducts. Some results indicate that instability arising from any of the layers may be critical, as indicated before. For example, Leijtens *et al.* have shown that the use of UV filters with devices containing a layer of mesoporous TiO_2 is necessary to reduce photodegradation at the oxide layer, and the replacement of this layer by Al_2O_3 delivers stable photocurrents for over 41 days at 5% efficiency from an initial power conversion efficiency (PCE) of 10%.[10]

The highest reported stability results under constant illumination include the use of mesoporous TiO_2 by Burschka *et al.* using a two-step deposition method where 80% of the initial efficiency is retained after 20 days from an initial 8%.[1] By removing spiro-Ometad and using a carbon protecting layer, Mei *et al.* have reported that the stability is enhanced to reach a constant efficiency of 10.5% after 41 days of steady illumination.[7] With the exception of the work by Mei *et al.*, in all reported cases, there is significant performance decay. In that work, the enhanced stability is attributed to the total exclusion of water into the device thanks to the presence of a 10 μm thick carbon layer back contact. On the other side of the stability race, we find flat heterojunction solar cells and, in this case, stability data are very scarce. Interestingly, other studies where devices have been encapsulated or have been measured in the glovebox do show significant device degradation.[10] Therefore, it is clear that other unknown degradation mechanisms different than those triggered by water are also taking place in most devices. Recently, Kaltenbrunner has reported enhanced stability with the use of Cr_2O_3 to shield the metal top contact from detrimental reactions with oxidizing and halide-forming iodide species.[11] The authors observed increased stability under ambient conditions, and reduced performance decay is ascribed to water penetration into the device in the time scale of some hours.

In this work, devices in the configuration ITO/PEDOT:PSS/$MAPbI_3$/PCBM/Metal are fully characterized before degradation and after degradation by simple constant illumination during 4 h in the glovebox. Two factors are responsible for device degradation: (1) degradation of the metal contact and (2) modification of the energy profile within the perovskite layer close to the contacts. The first factor can be suppressed by using a protective layer of Cr_2O_3. This work highlights the importance to further study how to stabilize the morphology and transport of iodide atoms through the bulk of the perovskite layer.

RESULTS AND DISCUSSION

Current Density–Voltage Curves. In this investigation, inverted flat solar cells in the configuration ITO/PEDOT:PSS/Perovskite/PCBM/Metal have been fabricated for different reasons. First of all, degradation of perovskite solar cells has been ascribed to the moisture present in the environment, and these devices work best when encapsulated.[7,9] Second, the use of an inverted configuration avoids the presence of a TiO_2 layer, which makes analysis more complex as electrical response will depend on the doping level and permittivity of the two semiconductor junction sides.[12] Finally, degradation features are more dramatic in the inverted configuration. A selection of different metals as cathode contacts has been tested in order to understand if degradation can be avoided.

Current density–voltage (J–V) curves have been measured at 1 sun light intensity conditions (1 kW/m^2). Representative curves are shown in Figure 1, and performance parameters are summarized in Table 1. As reported previously, high-performance devices can be prepared following a one-step preparation method using CH_3NH_3I and $PbCl_2$ (3:1) as precursor using low workfunction metals such as Ca or Al.[13] Full details are described in the Methods section. In this work, efficiencies of ~12% have been obtained for devices containing Ca or Al measured in the glovebox (J_{sc} = 18.4 mA/cm^{-2}, V_{oc} = 1.10 V, and FF = 60). Slightly lower efficiencies are obtained for devices containing Ag (8.7%), Au (7.3%), and Cr_2O_3/Cr (7.0%) mainly due to a reduction in V_{oc} and FF.

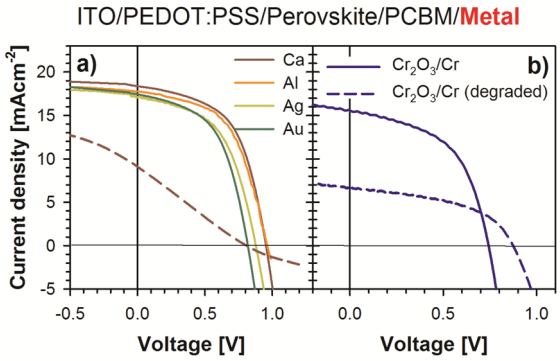

Figure 1. Current density–voltage curves of devices fabricated with different metal contacts measured at 1 sun light illumination. (a) Metals providing S-shape curves after degradation. (b) Contact containing Cr_2O_2/Cr does not show an S shape after degradation. Degraded devices are shown as broken lines.

Interestingly, in the absence of water, if the device is illuminated during 4 h at 1 sun light intensity, an S-shape curve evolves for most studied metals, which dramatically reduces the device efficiency, providing PCE of <1.7%. Selected J–V curves of degraded devices are shown in Figure 1 as broken lines. Only devices containing Cr_2O_2/Cr consistently show reduced degradation kinetics, as devices retain most of the initial FF, but the photocurrent is consistently reduced.

Bulk Properties of Perovskite Films. Current density curves with a S-shape are typically connected to degradation of the contacts.[14] However, in order to understand if degradation is also connected to a modification of the bulk material absorption and X-ray diffraction (XRD) measurements of pristine and degraded films were measured (Figure 2). Films in the configuration ITO/PEDOT:PSS/Perovskite/PCBM were illuminated during 4 h in the glovebox under 1 sun light intensity conditions to simulate the degradation conditions in devices. The absorption bands of pristine and degraded films are remarkably similar. Alternatively, XRD diffraction patterns differ, and modification of the XRD pattern takes place during illumination of the sample in the glovebox. In particular, the low fraction of the PbI_2 peak disappears, but peak intensities and ratios change as well as the fwhm, implicating a modification in the domain size.

DOI: 10.1021/acsnano.5b03687
ACS Nano 2016, 10, 218–224

Table 1. Device Performance Parameters for Devices Containing Different Cathode Contacts as a Function of Aging Conditions and Electrical Parameters Extracted from Capacitance–Voltage Measurements under Dark Conditions

contact	J_{sc} [mA/cm^2]	V_{oc} [V]	FF [%]	PCE [%]	n [×10^{16} cm^{-3}]	V_{fb} [V]	ΔV_{fb} [V]
Ca	18.39	1.10	60	12.14	1.2	1.00	
Ca	9.11	0.85	23	1.78	1.5	0.53	0.47
(degraded)					0.9	−0.40	0.93
Al	17.79	1.11	61	12.05	0.9	1. 06	
Ag	17.04	0.97	53	8.76	1.1	0.90	
Au	17.46	0.82	51	7.30	2.1	0.75	
Cr_2O_3/Cr	15.57	0.78	58	7.04	1.3	0.79	
Cr_2O_3/Cr	6.71	0.88	55	3.25	5.8	1.10	−0.31
(degraded)					5.1[a]	1.03[a]	0.07

[a]Measurement carried out at 1 sun light intensity.

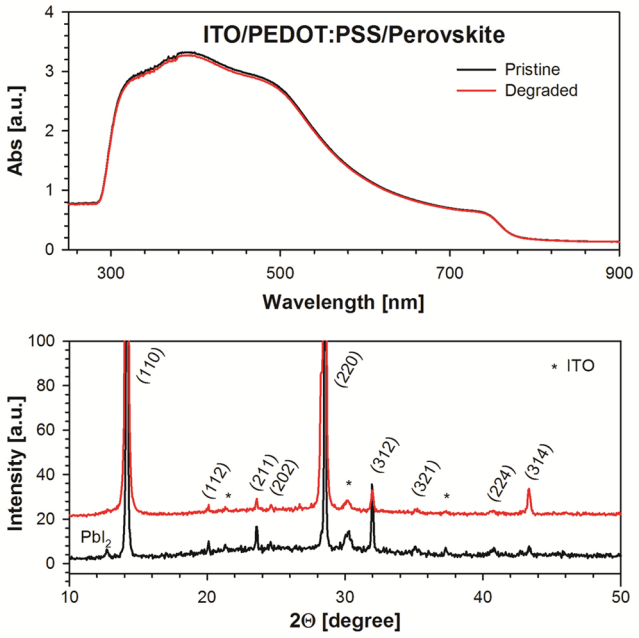

Figure 2. Bulk properties of pristine and degraded films in the configuration ITO/PEDOT:PSS/Perovskite/PCBM illuminated during 4 h in the glovebox under 1 sun light intensity conditions. Top: Absorbance spectra. Bottom: XRD diffraction pattern.

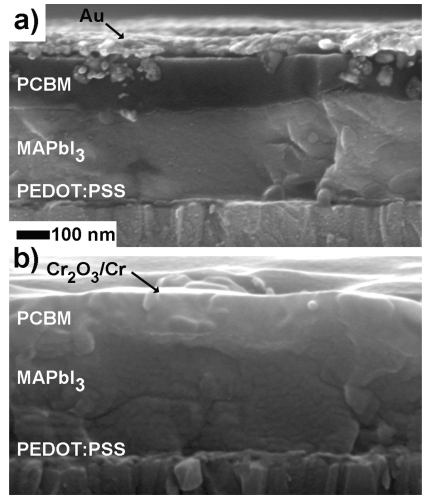

Figure 3. Scanning electron microscopy images of two representative degraded devices using the secondary electron detector (a) showing an S-shape J–V curve and (b) degraded device not showing an S-shape J–V curve.

Comparison of Degraded Devices by Scanning Electron Microscopy. In order to understand the origin of degradation in the absence of moisture and oxygen, degraded devices were analyzed by SEM microscopy. Two selected devices are shown in Figure 3 to illustrate two configurations behaving differently electrically. Configuration based on Ca, Al, Ag, or Au provides S-shape curves, and a representative image containing Au is shown in Figure 3a. From this secondary electrons image, it is clear that the gold contact is not smooth as it contains coarse grains not present in fresh devices (see Supporting Information). In addition, it is interesting to note that the PCBM/Au interface shows signs of delamination, and the $MAPbI_3$/PCBM interface is rather bright, pointing to a high presence of heavy metal atoms at the interface. This delamination does not seem to be a cleaving effect since fresh samples do not show delamination (see Supporting Information). Alternatively, degraded devices containing Cr_2O_3/Cr do not show an S shape in the J–V curve, and relatively high FFs are obtained. A representative degraded device is shown in Figure 3b, where it is clear that the Cr_2O_3/Cr surface is smooth. In addition, interfaces close to the cathode are difficult to differentiate. All together, this suggests that Cr_2O_3/Cr clearly protects the cathode contact. For data completeness, a comparison of fresh and aged devices using both secondary and backscattered electrons is shown as Supporting Information.

Capacitance–Voltage Measurements: Mott–Schottky Analysis. Capacitance–voltage measurement is a very useful technique at discerning between effects taking place at the bulk of active layer and those occurring at the interfaces with the outer contacts in photovoltaic devices.[12,15] The reason is that measured doping densities will depend on the bulk properties of the layer and flat-band potential values (V_{fb}) on energy equilibration at the contacts. In addition, capacitance measured at negative voltage under full depletion provides information on the dielectric constant of the material, and this is an intrinsic property of the bulk material. In a typical measurement, a DC voltage is applied under dark conditions and a small AC perturbation (typically at 10 kHz to 1 kHz) is overimposed. The differential current output is measured, and the DC voltage is swept over a wide range (*i.e.*, −1 V to +1 V). The measured intermediate capacitance is related to the width of the depletion zone, corresponding to a Schottky barrier at the cathode, as supported by Kelvin probe measurements.[12] At reverse bias full depletion occurs and corresponds to a geometric capacitance determined by the dielectric constant of the perovskite layer (Figure 4a). Full depletion of the perovskite at 0 V is observed,

DOI: 10.1021/acsnano.5b03687
ACS Nano 2016, 10, 218–224

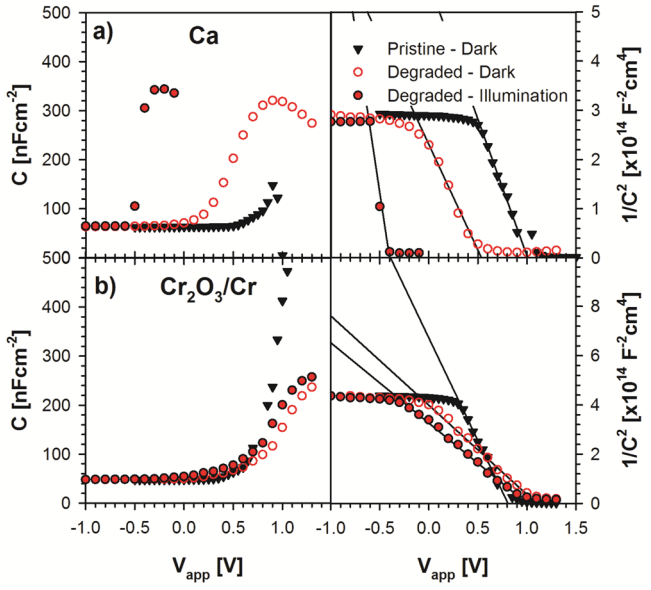

Figure 4. (a) Capacitance−voltage measurements of pristine and degraded devices carried out at 10 kHz. (b) Mott−Schottky plot of data shown in (a).

and taking into account that the thickness of the perovskite layer is about 300 nm, a relative dielectric constant for the perovskite (ε_{PVK}) of 21.2 has been found from the capacitance of fresh devices. The depletion zone decreases at positive bias voltage, and as a consequence, the capacitance increases (see Figure 4a); by plotting $C^{-2}(V)$, a straight line is observed (Figure 4).[16] The slope of the straight line is related to measurable p-doping density of electrical defects. In the current case, we expect some differences between fresh and degraded devices since the XRD patterns change during illumination, as previously described, and morphology is related with the defect density.

Two representative case examples are shown in Figure 4 for devices showing an S-shape after device degradation containing Ca contact (Figure 4a) and other devices retaining the initial FF containing Cr_2O_3/Cr (Figure 4b). The obtained doping levels of 10^{16} cm^{-3} (Table 1) are well in agreement with our previously published results.[12] On the other hand, the intercept with the x-axis provides information on the flat-band potential V_{fb}, defined as the applied voltage bias required to produce flat bands in the semiconductor. Note that V_{fb} is not actually the built-in potential (V_{bi}), as this last quantity also takes into account the presence of dipoles at the perovskite/cathode interface.

When data (Table 1) from fresh and degraded devices containing Ca metal are compared, a slight increase in doping density is observed, 1.06×10^{16} and 1.55×10^{16} cm^{-3}, respectively. This feature suggests that the bulk properties of the perovskite layer are not significantly being modified, pointing to interfacial degradation between the perovskite layer and the outer contacts for Ca-containing devices. In addition, we observe that the dielectric capacitance attributed to the bulk properties of the perovskite at negative voltage remains constant. Alternatively, a shift in the V_{fb} of 0.47 V is observed for devices containing Ca toward negative values from 1.00 to 0.53 V and this is a clear sign that the energetic properties at the interface between the cathode and the perovskite have dramatically been modified. More importantly, when we compare a degraded sample measured under dark conditions and under illumination, a shift in V_{fb} of about 0.93 V is observed that results in negative flat-band values. This is a clear sign of generation of a light-induced dipole at the cathode interface as a consequence of charge accumulation of photogenerated carriers at the perovskite/cathode interface. The same effect has been previously reported for organic PCBM:P3HT solar cells.[17] Impedance spectroscopy measurements were carried out on degraded devices showing $J-V$ curves with an S-shape (see Supporting Information). An additional resistance with magnitude dependent on the applied voltage correlates with the shape of the $J-V$ curve. This resistance is only observed for the degraded device, and it is relatively low and constant at negative values when the photocurrent is high but sharply increases at voltages more positive than −0.2 V when the photocurrent is low. This result points to an issue related with the extraction of carriers at the contact.

A remarkable increase in doping density is observed for degraded devices containing Cr_2O_3/Cr increasing from 1.3×10^{16} and 5.8×10^{16} cm^{-3}, in agreement with modification of the perovskite layer (see XRD results). This increase in doping density will have an effect on the energy equilibration at the cathode contact, as will be described below. For this reason, a degraded sample containing Cr_2O_3/Cr contact shows an increase in V_{fb}, again pointing to a modification in the energetic of all the elements involved at the cathode interface. Importantly, no shift in V_{fb} is observed when measurements in the dark and under illumination are compared. The additional resistance observed for devices containing a reactive metal is not observed for Cr_2O_3/Cr contacts.

Electrical Model. A general electrical model to understand contact equilibration in photovoltaic devices needs to account for the difference in work functions between the contacts, Φ, and the Fermi level of the active layer, E_F, shown in Figure 5a. Based on previous results, here we assume that the anode forms an ohmic contact with the perovskite active layer, in such a way that the energy equilibration to equalize the Fermi levels occurs predominantly at the contact $MAPbI_3$/PCBM. The potential drop associated with equilibration is generally divided into two contributions, as shown in Figure 5b: a spatially extended band bending (V_{fb}) in the bulk of the semiconductor, and a voltage drop at the interface by generation of a dipole layer (Δ/q), where Δ is the step of the vacuum level. Thus, the flat-band potential is given by the expression[15,18]

$$qV_{fb} = E_F - \Phi_c - \Delta \quad (1)$$

The presence of a dipole at the contact interface implies a net formation of charge separation across the interface, for example, if electron charge is donated from the contact to acceptor states at the surface of the semiconductor.[18] We have previously shown using Kelvin probe force microscopy (KPFM) that the magnitude of this dipole is almost negligible for highly performing perovskite solar cells.[12] The differences in work function between cathode and Fermi level of the perovskite is accommodated in the heterojunction with a depletion zone reaching about 300 nm of the perovskite layer.

While in a good performing device the dipole is very small, the evidence presented in the previous sections about the Mott−Schottky analysis and interfacial resistance indicates that in degraded devices a large dipole is generated at the cathode/perovskite interface, and this situation is indicated in Figure 5c.

DOI: 10.1021/acsnano.5b03687
ACS Nano 2016, 10, 218−224

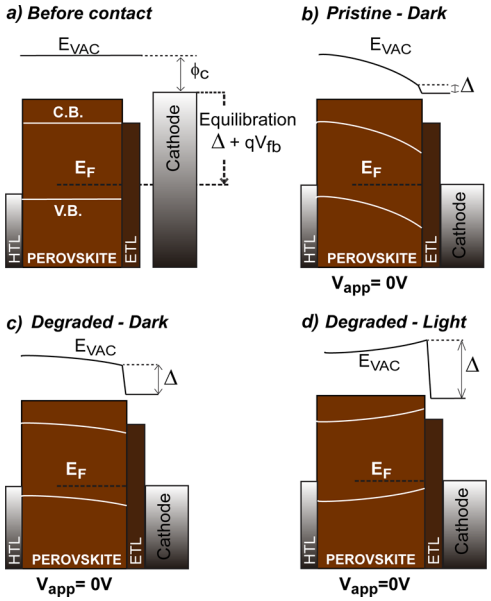

Figure 5. Energy level diagram of devices that show an S-shape $J-V$ curve (a) before contact equilibration, (b) after contact equilibration for a fresh device under dark conditions, and after contact equilibration for a degraded device under dark (c) and illumination (d) conditions. HTL and ETL are hole transport layer and electron transport layer, respectively. Formation of an interfacial dipole for the degraded device reduces the measured V_{fb}, and the band in the electrical profile in the bulk of the perovskite layer is reversed, hindering an efficient extraction of electrons. The magnitude of the dipole is magnified by accumulation of photogenerated carriers at the perovskite/cathode interface.

The diagram shows that the presence of such a dipole reduces the required applied potential to provide flat bands and thus the measured V_{fb} is lower. From the point of view of photovoltaic operation, it is clear that the efficient charge collection induced by the electrical field present in Figure 5b is eroded in Figure 5c. Under illumination conditions, the magnitude of the dipole is magnified by accumulation of photogenerated carriers at the perovskite/cathode interface. This effect has been previously described in terms of the charging of the interface.[17] It produces an energy profile inversion which impedes efficient charge extraction by the cathode, which is responsible for the S-shape curve.[14] Alternatively, for Cr_2O_3/Cr-containing devices, the doping density increases, increasing the value of E_F, and this will induce an increase in V_{fb} following eq 1.

Origin of Performance Degradation. Identification of the precise interfacial reactions that actually cause the large dipole at the perovskite/cathode interface, limiting the device performance, is a complex problem of compositional analysis at the nanoscale that is beyond the scope of this work. Nevertheless, the fact that the use of chromium provides a totally different degradation behavior points to corrosion of the metal contact for Ca, Al, Ag, and Au as observed in SEM images in Figure 3. Importantly, recently it has been recognized that significant ionic conduction takes place in hybrid lead iodide perovskite that gives rise to accumulation of net charge at one or both contacts.[19−21] A first-principles calculation finds that that iodide vacancies and interstitials may easily diffuse across the perovskite crystal.[22] Hence, under illumination, the internal field shown in Figure 5c may produce the displacement of excess iodide atoms to the cathode, neutralizing the existing barrier. Ion migration as such is a reversible effect that does not account for permanent degradation, process I in Figure 6.

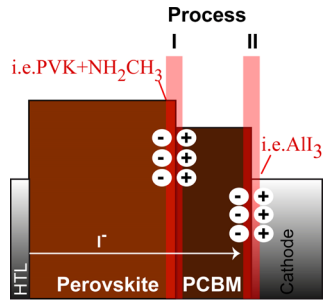

Figure 6. Feasible hypothesis that could potentially give rise to external cathode contact degradation.

However, metals would be prone to react with I^- ions, producing irreversible degradation of the interface with generation of insulating metal-iodide materials, process II in Figure 6. In addition, the evaporated metal could also diffuse through the thin layer of PCBM and I^- would not necessarily need to diffuse thorough the entire PCBM layer. Noble metals such as Au also lead to corrosion at the interface level under oxidative stress, and similar results are also observed here.[23] Note that in this case positive charges would be generated at the anode side, but this would be better compensated by the PEDOT:PSS as this is a solid state polyelectrolyte. Unlike with cathode contact, the effect of this additional charge on PEDOT:PSS would be to increase of the conductivity of the layer. In both processes, an insulating layer would be formed at the interface, which under illumination would generate charge accumulation at the interfaces, inducing the generation of a dipole either at I or II and would account for the observed measurements. Alternatively, Cr_2O_3 is known to withstand oxidative corrosion very well. Recently, it has been reported that Cr_2O_3 efficiently shields the top metal from detrimental reactions with oxidizing and halide-forming iodide species.[11] Using this protective layer, the reduction in photocurrent and increase in photovoltage are related to the ion migration itself (process I), which reversibly modifies the energetic landscape at the perovskite/PCBM contact.

CONCLUSIONS

In this work, we have studied the degradation of flat heterojunction solar cells fabricated in the inverted configuration. We have demonstrated that, in the absence of water, which is believed to be the major degradation source for these types of devices, reactivity of the perovskite with the cathode contact is the major degradation pathway for most metals. If the cathode contact is protected with Cr_2O_3/Cr, new features appear during degradation which are due to modification of the energy bands close to the contacts. The results presented in this article highlight the importance to study the use of protecting layers to avoid the chemical reactivity of the perovskite with the external contacts. Further work is needed to suppress the ionic conductivity within the perovskite layer, as this modifies the performance of flat heterojunction perovskite solar cells during operation conditions.

METHODS

Device preparation was carried out according to previously described methods, and a brief summary is provided here.[13] A solution

DOI: 10.1021/acsnano.5b03687
ACS Nano 2016, 10, 218−224

containing $PbCl_2/CH_3NH_3I$ (1:3) in *N*,*N*-dimethylformamide (0.8M) was spin-coated at 1500 rpm onto the poly(3,4-ethylenedioxythiophene):polystyrenesulfonate (PEDOT:PSS) layer. The precursor film was annealed at 90 °C for 2 h in ambient air (humidity of 35−65%). After being annealed, the perovskite films were transferred into nitrogen glovebox. A 2% phenyl-C61-butyric acid methyl ester ($PC_{70}BM$) in chlorobenzene solution was coated onto the perovskite layer at 1000 rpm. Top metals were thermally evaporated with a base pressure of 6×10^{-6} mbar. Deposition of chromium was carried out as in ref 11. Efficiencies were measured using encapsulated devices in air using a solar simulator, and identical devices not encapsulated were measured by capacitance voltage in the glovebox at <0.1 ppm of O_2 and water.

J−*V* curves were measured using a solar simulator with the light intensity adjusted using a calibrated Si solar cell. Measurements were carried out at a sweep rate of 50 mV/s with very small hysteresis observed. Capacitance−voltage and impedance spectroscopy measurements were performed using an Autolab potentiostat (model PGSTAT30) equipped with a frequency analyzer module. A small voltage perturbation (20 mV rms) was applied at frequencies from 10 kHz for capacitance−voltage. Capacitance−voltage measurements were carried out either in the dark or at 1 sun light illumination. Small sample-to-sample variation was observed in doping densities ($\pm 0.8 \times 10^{16}$ cm^{-3}) and V_{fb} (± 0.10 V) for 20 independent devices fabricated using the same process.

Films for absorption and XRD measurements were prepared as those in devices, but the top contact was not evaporated. The degradation experiment for those films was carried out in a glovebox using 1 sun light intensity during a period of 4 h. Absorption measurements were carried out with a Cary 300 Bio spectrophotometer. Powder XRD analysis was performed with a thin film X-ray diffractometer (D4 Endeavor, Bruker-AXS) with Cu Kα radiation.

ASSOCIATED CONTENT

Supporting Information

The Supporting Information is available free of charge on the ACS Publications website at DOI: 10.1021/acsnano.5b03687.

Complete comparison of SEM images of fresh and degraded devices and additional impedance spectroscopy data (PDF)

AUTHOR INFORMATION

Corresponding Authors

*E-mail: aguerrer@uji.es.

*E-mail: yangy@ucla.edu.

Notes

The authors declare no competing financial interest.

ACKNOWLEDGMENTS

This work was partially supported by Generalitat Valenciana (project ISIC/2012/008 Institute of Nanotechnologies for Clean Energies) and the Spanish Ministerio de Economía y Competitividad (MINECO) project MAT2013-47192-C3-1-R; and grants from U.S. Air Force of Scientific Research (FA9550-12-1-0074) and National Science Foundation (ECCS-1509955). A.G. would like to thank the Spanish Ministerio de Economía y Competitividad for a Ramón y Cajal Fellowship (RYC-2014-16809). We thank SCIC from UJI for support on use of the scanning electron microscope.

REFERENCES

(1) Burschka, J.; Pellet, N.; Moon, S.-J.; Humphry-Baker, R.; Gao, P.; Nazeeruddin, M. K.; Gratzel, M. Sequential Deposition as a Route to High-performance Perovskite-sensitized Solar Cells. *Nature* **2013**, *499*, 316−319.

(2) Lee, M. M.; Teuscher, J.; Miyasaka, T.; Murakami, T. N.; Snaith, H. J. Efficient Hybrid Solar Cells Based on Meso-Superstructured Organometal Halide Perovskites. *Science* **2012**, *338*, 643−647.

(3) Zhou, H.; Chen, Q.; Li, G.; Luo, S.; Song, T.-b.; Duan, H.-S.; Hong, Z.; You, J.; Liu, Y.; Yang, Y. Interface Engineering of Highly Efficient Perovskite Solar Cells. *Science* **2014**, *345*, 542−546.

(4) Green, M. A.; Emery, K.; Hishikawa, Y.; Warta, W.; Dunlop, E. D. Solar Cell Efficiency Tables (Version 45). *Prog. Photovoltaics* **2015**, *23*, 1−9.

(5) Kim, J. H.; Williams, S. T.; Cho, N.; Chueh, C.-C.; Jen, A. K. Y. Enhanced Environmental Stability of Planar Heterojunction Perovskite Solar Cells Based on Blade-Coating. *Adv. Energy Mater.* **2015**, *5*, 1401229.

(6) Hwang, K.; Jung, Y.-S.; Heo, Y.-J.; Scholes, F. H.; Watkins, S. E.; Subbiah, J.; Jones, D. J.; Kim, D.-Y.; Vak, D. Toward Large Scale Roll-to-Roll Production of Fully Printed Perovskite Solar Cells. *Adv. Mater.* **2015**, *27*, 1241−1247.

(7) Mei, A.; Li, X.; Liu, L.; Ku, Z.; Liu, T.; Rong, Y.; Xu, M.; Hu, M.; Chen, J.; et al. A Hole-conductor−free, Fully Printable Mesoscopic Perovskite Solar Cell with High Stability. *Science* **2014**, *345*, 295−298.

(8) Chen, Q.; Zhou, H.; Hong, Z.; Luo, S.; Duan, H.-S.; Wang, H.-H.; Liu, Y.; Li, G.; Yang, Y. Planar Heterojunction Perovskite Solar Cells *via* Vapor-Assisted Solution Process. *J. Am. Chem. Soc.* **2014**, *136*, 622−625.

(9) Frost, J. M.; Butler, K. T.; Brivio, F.; Hendon, C. H.; van Schilfgaarde, M.; Walsh, A. Atomistic Origins of High-Performance in Hybrid Halide Perovskite Solar Cells. *Nano Lett.* **2014**, *14*, 2584−2590.

(10) Leijtens, T.; Eperon, G. E.; Pathak, S.; Abate, A.; Lee, M. M.; Snaith, H. J. Overcoming Ultraviolet Light Instability of Sensitized TiO_2 with Meso-Superstructured Organometal Tri-halide Perovskite Solar Cells. *Nat. Commun.* **2013**, *4*, 2885.

(11) Kaltenbrunner, M.; Adam, G.; Glowacki, E. D.; Drack, M.; Schwodiauer, R.; Leonat, L.; Apaydin, D. H.; Groiss, H.; Scharber, M. C. Flexible High Power-per-weight Perovskite Solar Cells with Chromium Oxide-Metal Contacts for Improved Stability in Air. *Nat. Mater.* **2015**, *14*, 1032−1039.

(12) Guerrero, A.; Juarez-Perez, E. J.; Bisquert, J.; Mora-Sero, I.; Garcia-Belmonte, G. Electrical Field Profile and Doping in Planar Lead Halide Perovskite Solar Cells. *Appl. Phys. Lett.* **2014**, *105*, 133902.

(13) You, J.; Yang, Y.; Hong, Z.; Song, T.-B.; Meng, L.; Liu, Y.; Jiang, C.; Zhou, H.; Chang, W.-H.; Li, G. Moisture Assisted Perovskite Film Growth for High Performance Solar Cells. *Appl. Phys. Lett.* **2014**, *105*, 183902.

(14) Guerrero, A.; Chambon, S.; Hirsch, L.; Garcia-Belmonte, G. Light-Modulated TiOx Interlayer Dipole and Contact Activation in Organic Solar Cell Cathodes. *Adv. Funct. Mater.* **2014**, *24*, 6234−6240.

(15) Guerrero, A.; Dörling, B.; Ripolles-Sanchis, T.; Aghamohammadi, M.; Barrena, E.; Campoy-Quiles, M.; Garcia-Belmonte, G. Interplay between Fullerene Surface Coverage and Contact Selectivity of Cathode Interfaces in Organic Solar Cells. *ACS Nano* **2013**, *7*, 4637−4646.

(16) Boix, P. P.; Garcia-Belmonte, G.; Munecas, U.; Neophytou, M.; Waldauf, C.; Pacios, R. Determination of Gap Defect States in Organic Bulk Heterojunction Solar Cells from Capacitance Measurements. *Appl. Phys. Lett.* **2009**, *95*, 233302.

(17) Bisquert, J.; Garcia-Belmonte, G.; Munar, A.; Sessolo, M.; Soriano, A.; Bolink, H. J. Band Unpinning and Photovoltaic Model for P3HT:PCBM Organic Bulk Heterojunctions Under Illumination. *Chem. Phys. Lett.* **2008**, *465*, 57−62.

(18) Guerrero, A.; Marchesi, L. F.; Boix, P. P.; Ruiz-Raga, S.; Ripolles-Sanchis, T.; Garcia-Belmonte, G.; Bisquert, J. How the Charge-Neutrality Level of Interface States Controls Energy Level Alignment in Cathode Contacts of Organic Bulk-Heterojunction Solar Cells. *ACS Nano* **2012**, *6*, 3453−3460.

(19) Xiao, Z.; Yuan, Y.; Shao, Y.; Wang, Q.; Dong, Q.; Bi, C.; Sharma, P.; Gruverman, A.; Huang, J. Giant Switchable Photovoltaic Effect in Organometal Trihalide Perovskite Devices. *Nat. Mater.* **2015**, *14*, 193−198.

(20) Yang, T.-Y.; Gregori, G.; Pellet, N.; Grätzel, M.; Maier, J. The Significance of Ion Conduction in a Hybrid Organic–Inorganic Lead-Iodide-Based Perovskite Photosensitizer. *Angew. Chem., Int. Ed.* **2015**, *54*, 7905–7910.
(21) Almora, O.; Zarazua, I.; Mas-Marza, E.; Mora-Sero, I.; Bisquert, J.; Garcia-Belmonte, G. Capacitive Dark Currents, Hysteresis, and Electrode Polarization in Lead Halide Perovskite Solar Cells. *J. Phys. Chem. Lett.* **2015**, *6*, 1645–1652.
(22) Azpiroz, J. M.; Mosconi, E.; Bisquert, J.; De Angelis, F. Defects Migration in Methylammonium Lead Iodide and their Role in Perovskite Solar Cells Operation. *Energy Environ. Sci.* **2015**, *8*, 2118.
(23) Verdingovas, V.; Müller, L.; Jellesen, M. S.; Grumsen, F. B.; Ambat, R. Effect of Iodine on the Corrosion of Au–Al Wire Bonds. *Corros. Sci.* **2015**, *97*, 161–171.

DOI: 10.1021/acsnano.5b03687
ACS Nano 2016, 10, 218–224